Advances in Intelligent Systems Research, volume 175
2nd International Conference on Industry 4.0 and Artificial Intelligence (ICIAI 2021)

Polypyrrole-Metal Oxide-Carbon Nanocomposite Films Corrosion Enhancement on Industrial Steel

Inshad Jum'h[1*], Yousef Al-Abdallat[2], Ehab M. AlShamaileh[3], Mohammad D. AL-Tahat[2], Ahmad Telfah[4]

1School of Basic Sciences and Humanities, German Jordanian University (GJU), Amman 11180, Jordan

2 Industrial Engineering Department, University of Jordan (UJ), Amman 11942, Jordan

3Department of Physical Sciences, Jordan University of Science & Technology, Irbid 22110, Jordan

3Department of Chemistry, The University of Jordan, Amman 11942, Jordan

4LeibnizInstitutfürAnalytischeWissenschaften - ISAS - e.V. 44139 Dortmund, Germany

[*]Corresponding author. Email: inshad.yousef@gju.edu.jo

ABSTRACT

Nanocomposite films of polypyrrole (PPy) doped with zinc oxide nanoparticles (ZnO NPs), silica nanoparticles (SiO_2 NPs), and carbon were synthesized using electrochemical technique. These films were proposed as an anticorrosion agent and tested on industrial steel samples. The films and the dopant nanoparticles (ZnO NPs and SiO_2 NPs) were investigated by employing Scanning electron microscope (SEM) and Nanoparticle tracking analysis (NTA) to determine their morphologyy and size distributions. The anticorrosion properties of PPy, PPy/ZnO, PPy/ZnO/carbon and PPy/ZnO/carbon/SiO_2 nanocomposites coated on industrial steel within corrosive solutions was tested with a potentiodynamic method, generated Tafel plots were interpreted. The best performance as an anticorrosion agent for industrial steel was the PPy composite containing ZnO/carbon nanoparticles, which reduced corrosion rate by 77% compared to uncoated steel. In this work, it was demonstrated that the coating composed of polypyrrole-metal oxide-carbon Nanocomposite was highly efficient in protecting the Industrial steel compared to the PPy film. PPy/ZnO/carbon nanocomposite exhibited the highest anticorrosion efficiency.

Keywords: *Nanocomposite films, Polypyrrole, Zinc oxide nanoparticles, Silica nanoparticles, Corrosion protection.*

1. INTRODUCTION

Corrosion of metal surfaces is a significant issue for metallic constructions, including storage tanks, pipelines, and bridges. The corrosion degree increases significantly when exposed to an aggressive environment, such as seawater [1, 2]. Corrosion is a natural process that occurs to metals. Due to chemical and electrochemical reactions with their surroundings, it transforms them into more chemically stable compounds such as metal oxide, metal hydroxide, or metal sulfidic [3, 4]. For example, rusting is a process in which metals undergo electrochemical oxidation [5]. Corrosion is a significant issue, with a considerable expense associated with it [6].

Corrosion protective coatings are a simple and scalable technology that inhibits electrons from exchanging in an electrochemical reaction by forming a layer between the substrate and the hostile liquid [7]. Hybrid organic-inorganic coatings are utilized to protect the surfaces of some materials [8]. The primary function of hybrid organic-inorganic coatings is to increase output by preventing oxygen from reaching the metal surface [9].

Conductive polymers, such as polypyrrole (PPy) and polyaniline (PANI), are some of the most effective coatings for providing good corrosion protection [10]. Additionally, conductive polymers are organic materials, implying they pose no risk to human health or the environment [11].

The enhancement of the corrosion protection mechanism was investigated in this research using four distinct combination coatings: PPy, PPy-ZnO NPs, PPy-ZnO NPs-Carbon, and PPy-ZnO NPs-Carbon-SiO_2 NPs. Metal oxides using as dopant materials in the conductive polymer due to its inherent properties, which enhanced the protective performance of the conductive polymers [12]. ZnO-NPs, SiO_2-NPs, and carbons were used as dopant materials in conductive polymers to enhanced the protective performance [13]. In this research, we will investigate the protective performance for co-doping process of these dopant in polypyrrole (PPy). Nanoparticle tracking analysis (NTA), scanning electron microscopy (SEM), and energy-dispersive X-ray microscopy (EDX) were used to characterize ZnO and SiO2 nanoparticles (EDX). The corrosion resistance of the sample was determined using the Tafel polarization plot.

2. EXPERIMENTAL PROCEDURE

2.1 Synthesis of Zinc Oxide Nanoparticles (ZnO NPs)

Two grams of Zinc Acetate Dihydrate Zn (CH3CO2)2.2H2O were dissolved in twenty milliliters of 100% ethanol. 0.5 g sodium hydroxide (NaOH) was dissolved in 20 ml 100% ethanol separately. Later, the produced NaOH solution was gradually and gently mixed into the Zinc Acetate Dehydrate-ethanol solution while stirring continuously for 30 minutes. The resulting solution was kept at 70°C in a water bath for 2.5 hours. To eliminate contaminants from the obtained ZnO NPs, they were washed three times with ethanol and distilled water and dried in air at 50°C for 24 hours. Finally, ZnO NPs were collected in powder form and dried at a approximately temperature (100°C) [14].

2.2 Preparation of Silicon Dioxide Nanoparticles (SiO_2 NPs)

The SiO_2 NPs were synthesized by diluting 66 ml ethanol with 4 ml water and adding 1 g sodium hydroxide (NaOH) dissolved in ethanol. A suitable amount of time was allowed to produce homogeneity by adding 4 ml of tetraethyl orthosilicate ($SiC_8H_{20}O_4$) to the latter mixture for 15 minutes at 25 °C (water bath) and then 4 ml of NaOH in an ethanol solution (30 minutes). The resultant solution was centrifuged for 15 minutes, and the water was easily removed once the SiO_2 precipitated [15,16].

2.3 Coating Process

An electrochemical coating process was used to create films on mild steel specimens. Four different solutions have been prepared. The first solution was prepared by sonicating 0.1 g of Polypyrrole (PPy) for an hour at room temperature in 30 mL of Ethelene glycol. Sonicating 0.1 g PPy made a second solution, and 0.01 g produced ZnO NPs for an hour at room temperature in 30 ml Ethelene glycol. The third solution was sonicated for an hour at room temperature using 0.1 g PPy, 0.01 g produced ZnO NPs, and 0.01 g carbon nanotube in 30 ml Ethelene glycol. The fourth solution is the same as the third, except that 0.01 g of the SiO2 NPs generated are added. The electrochemical reaction occurs in an electrochemical cell, which is used to induce a non-spontaneous redox reaction using electrical energy that is typically used to break down chemical compounds [17]. This approach involves attaching the metal to a more anodic metal (Zinc), which changes it to a cathodic state and prevents corrosion. The stainless-steel specimens were coated with the four solutions and used as an anode in an electrochemical cell, allowing the coating material to stick to the anode by losing electrons from its valence shell, causing the electrolytes to form a thin film around it and coat it. Electrochemical deposition at an applied voltage of 8 V for 24 hours was used to prepare Polypyrrol/ZnO-NPs, Polypyrrole/ZnO-NPs/carbon, and Polypyrrole/ZnO-NPs/carbon/SiO2-NPs samples for anti-corrosion tests.

2.4 Potentiodynamic polarization measurement (PDP)

A VoltaLab PGZ 100 potentiostat was used in a double-wall three-electrode glass cell to detect PDP corrosion. The surface area of stainless-steel specimens exposed to corrosion was reduced to 6 cm2 before conducting potentiodynamic polarization tests. The tests were performed at room temperature (297 K). A saturated AgCl electrode was employed as a reference electrode, and a graphite electrode was used as an auxiliary electrode. Sodium chloride, at a concentration of 3.5 %, was used in the electrolyte solution. Regarding the open-circuit voltage, polarization curves were obtained at 10 mV/s from the cathode potential of -800 mV to the anode potential of -420 mV. (OCP). The corrosion potential (E-corr) and current densities (I-corr) were extrapolated from the Tafel graphs.

3. Results and Discussion

3.1 NTA, SEM and EDX results for ZnO NPs and SiO_2 NPs

Figure 1A illustrates the NTA results for the ZnO NPs. The image depicts results from the ZnO NPs experiment over particle sizes ranging from 0 to 199 nm, with concentrations measured in [106 particles/ml] at a temperature of 19.9 °C.

As shown in Figure 1A, the particle size spans from 40 nm to around 400 nm, the concentration is 106 particles/ml, and the particle size increases very slightly, virtually negligibly, at approximately 42 nm. The maximum concentration of 3.2261x106 particles/ml is observed with a particle size of 172 nm. At 172 nm, the concentration decreases until it reaches 313 nm, at which point the concentration decreases at a prolonged rate until it hits zero at 1397 nm particle size. We can deduce that the prevalent sizes vary between 42 and 300 nm. The most concentrated form is nanoparticles with a diameter of 172 nm. The SEM micrograph pictures in Figure 1B indicate the presence of ZnO NPs with spherical structures and the particles' aggregation. The particles should have aggregated due to their large specific surface area and high surface energy, which are characteristic of ZnO nanoparticles [18].

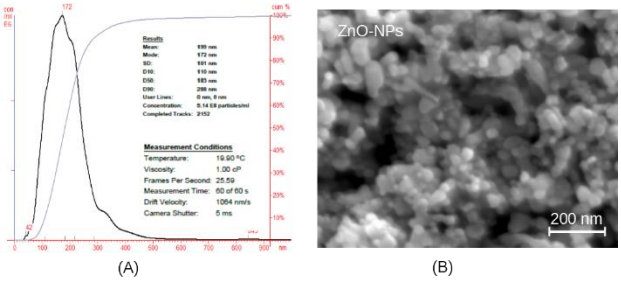

Figure 1: (A) NTA of 20% ZnO NPs dissolved in H_2O 1 mg in 1 ml concentration as well as the results and the measurement conditions. Data and plot obtained using NanoSight LM10 NTA instrument and NanoSight LM10 NTA software v3.00. (B)The SEM micrographs for ZnO NPs.

The NTA experiment was carried out on SiO_2 NPs at a temperature of 21.3 °C (Figure 2A) and a concentration of 106 particles/ml. The concentration gradually rises to a maximum of 0.1952x106 particles/ml with a particle size of 131 nm. The generated SEM micrographs (SiO2 NPs at two different magnifications) show a spherical morphology as the main structure, demonstrating the synthesis of SiO_2 nanostructures with limited agglomeration (Figure 2b).

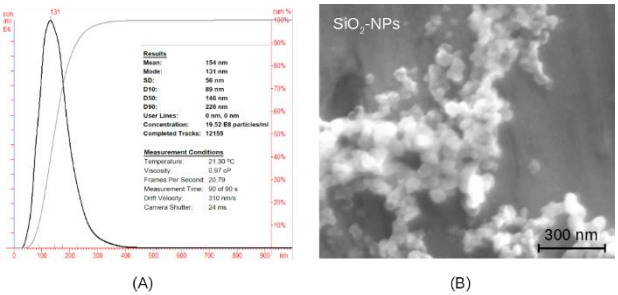

Figure 2: (A) NTA of 20% SiO_2 NPs dissolved in H_2O 1mg in 1ml concentration as well as the results and the measurement conditions. Data and plot obtained using NanoSight LM10 NTA instrument and NanoSight LM10 NTA software v3.00. **(B)** SEM micrographs of SiO_2 NPs.

3.2 PPy/nanocomposite surface Analysis Studies

SEM pictures of PPy films on steel, including a variety of nanocomposites, are shown in Figure 3. For this electrochemical deposition process, the flat surface of the PPy film is expected [19]. The various nanocomposite/PPy coated steels (Figure 3B, C, and D) exhibit a coarse-grained structure with aggregate development. These findings corroborate those on polarization and impedance.

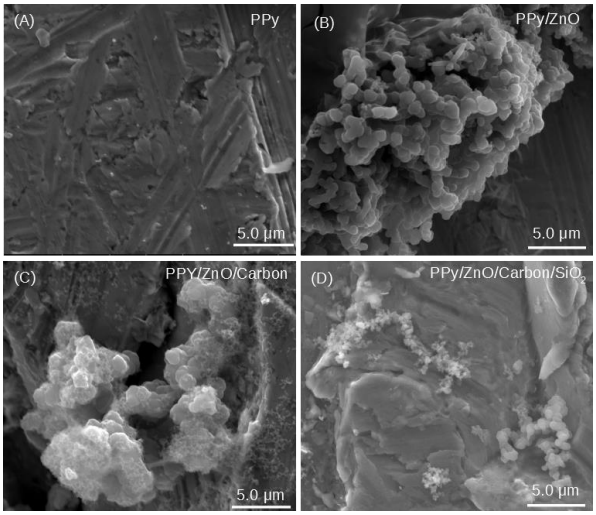

Figure 3: SEM micrographs of the pure PPy on steel and the nanocomposite films.

3.3 Potentiodynamic polarization measurements

The corrosion inhibition was studied using the Tafel polarization plot in NaCl media with an Ag/AgCl reference electrode. Figures 4 and 5 show Tafel plots for blank steel versus specimens coated with steel-PPy, steel-PPy-ZnO, steel-PPy-ZnO-carbon, and steel-PPy-ZnO-carbon-SiO_2 in NaCl solutions. Table 1 shows the electrochemical parameters obtained from Tafel curves, such as corrosion potential (E_corr), corrosion current density (I_corr), and cathodic and anodic Tafel slopes (β_c, β_a). The corrosion current density can be calculated by extrapolating the cathodic term to the corrosion potential. The following equation [20, 21] gives the inhibition efficiency (E_p %):

$$E_p\% = \frac{I^0_{corr} - I_{corr}}{I^0_{corr}} \times 100$$

I_corr represents the corrosion current density with the inhibitor, and I_corr^0 represents the corrosion current density without the inhibitor. Figure 4 shows that all coated samples have lower values of internal current, implying that uncoated steel has a lower corrosion rate. Steel-PPy-ZnO-carbon coated sample has the lowest internal current value, indicating the lowest corrosion rate of all coated samples. According to Table 1, all coated samples have a lower corrosion rate than uncoated steel (78.5 µm/year). Steel-PPy, for example, has a

Table 1. Table 1: Tafel parameters results of the tested specimens.

Specimen	Steel	Steel + PPy	Steel + PPy +ZnO	Steel + PPy +ZnO + Carbon	Steel + PPy +ZnO + Carbon + SiO_2
Corrosion potential (E_{corr}) [mV]	- 561.3	- 679.5	- 445.5	- 513.6	- 557.6
Rp [kohm/cm²]	1.75	2.44	5.88	5.99	2.42
Corrosion current densities (I_{corr}) [µA/cm²]	6.7118	4.2444	2.2173	1.5745	4.1648
βa [mV]	52.3	56.6	59.4	39.7	53.8
βc [mV]	- 89.3	- 64.1	- 105.7	- 75.2	- 66.3
Corrosion rate [µm/year]	78.5	49.64	25.93	18.41	48.71
Inhibition Efficiency [E_P%]	-	37	67	77	38

corrosion rate of 49.64 µm/year with an inhibition efficiency of 37%, Steel-PPy-ZnO has a corrosion rate of 25.93 µm/year with an inhibition efficiency of 67%, Steel-PPy-ZnO-Carbon has a corrosion rate of 18.41 m/year with an inhibition efficiency of 77%, and Steel-PPy-ZnO-carbon-SiO_2 has a corrosion rate of 48 µm/year.

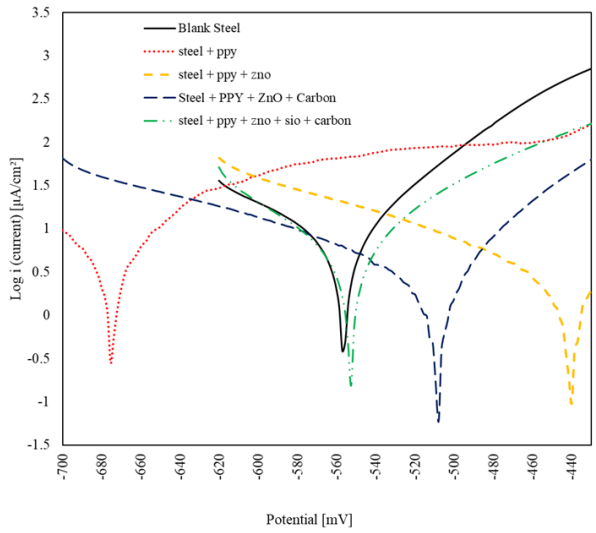

Figure 4: Tafel plot of the blank steel against specimens coated with steel-PPy (dotted red line), steel-PPy-ZnO (dashed dotted green line), steel-PPy-ZnO-carbon (dashed black line) and steel-PPy-ZnO-carbon-SiO_2 (dashed yellow line).

As illustrated for better comparison in Figure 5, the corrosion potential of the steel-PPy-ZnO-Carbon coated sample was changed to the anodic direction (E49 mV) in comparison to the blank steel. Additionally, the steel-PPy-ZnO-carbon coated sample's anodic Tafel slope was enhanced, indicating a considerable decrease in corrosion current [22]. Steel-PPy-ZnO-carbon (Table 1) is the best anti-corrosion agent among the four compositions tested, as the corrosion rate of steel decreased from 78.5 µm/year to 18.41 µm/year (77%) when coated with PPy-ZnO-Carbon. Additionally, inhibitors are divided into anodic, cathodic, and mixed types [23]. According to the literature [24-27], the inhibitors are either anodic or cathodic, indicating that the E_corr varies by more than 85 mV to the anode or cathode potential. In this work, the PPy-ZnO-Carbon coating altered the E_corr value by only 49 mV, indicating that this inhibitor acted as a mixed-type inhibitor with a proclivity for blocking surface-active sites on mild steel [28].

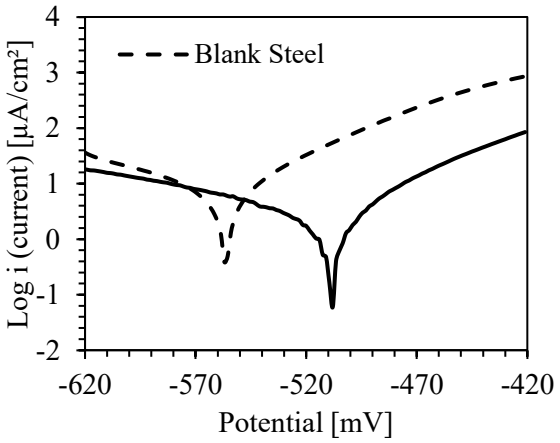

Figure 5: Tafel Plots of the blank steel and steel-PPy-ZnO-carbon specimens.

4. Conclusions

All PPy nanocomposite films exhibit lower internal current values than uncoated steel, implying a decreased corrosion rate. Coating steel with PPy, PPy-ZnO, or PPy-ZnO-carbon-SiO_2 reduces the steel's corrosion rate from 78.5 µm/year to 49.64 µm/year 25.93 µm/year, or 48.71 µm/year, respectively. However, steel-PPy-ZnO-carbon

is the most effective anti-corrosion agent among the four compositions studied, as the corrosion rate of steel decreased from 78.5 µm/year to 18.41 µm/year with a 77 % inhibitory efficacy. Additionally, the PPy-ZnO-Carbon coating modifies the E_corr by only 49 mV, indicating that this inhibitor worked as a mixed-type inhibitor with a proclivity for inhibiting mild steel surface-active sites.

Based on the results of this work, the conductive polymers such as PPy doped with metal oxide nanoparticles can play a significant role in being used as anticorrosive coating, therefore we recommend investigating other class of conductive polymers as polyaniline doped with dielectric nanoparticles such as polystyrene nanoparticles.

5. Table of Acronyms.

Abbreviation	**Description**
PPy	polypyrrole
SEM	Scanning electron microscope
NTA	Nanoparticle tracking analysis
ZnO	zinc oxide nanoparticles
SiO2	silica nanoparticles
PANI	polyaniline
Zn (CH3CO2)2.2H2O	Zinc Acetate Dihydrate
NaOH	sodium hydroxide
SiC8H20O4	tetraethyl orthosilicate
OCP	open-circuit The and
E-corr	corrosion potential
I-corr	current densities

5. References

[1] Z. Khoshkhou, M. Torkghashghaei, and A. R. Baboukani, "Corrosion inhibition of henna extract on carbon steel with hybrid coating TMSM-PMMA in HCL solution," *Open Journal of Synthesis Theory and Applications,* vol. 7, no. 01, p. 1, 2018.

[2] G. Polizos *et al.*, "Corrosion Behavior of Zinc–Nickel and Graphene Layered Structures on Steel Substrates," *Advanced Engineering Materials,* p. 1800949, 2019.

[3] G. Palanisamy, "Corrosion inhibitors," in *Corrosion Inhibitors*: Intechopen, 2019.

[4] U. Bharatiya, P. Gal, A. Agrawal, M. Shah, and A. Sircar, "Effect of corrosion on crude oil and natural gas pipeline with emphasis on prevention by ecofriendly corrosion inhibitors: A comprehensive review," *Journal of Bio-and Tribo-Corrosion,* vol. 5, no. 2, p. 35, 2019.

[5] Y. Hu *et al.*, "Electrochemical behaviors of anode materials and their performance for bauxite desulfurization," *Chinese Journal of Chemical Engineering,* vol. 27, no. 4, pp. 802-810, 2019.

[6] A. Goyal, H. S. Pouya, E. Ganjian, and P. Claisse, "A review of corrosion and protection of steel in concrete," *Arabian Journal for Science and Engineering,* vol. 43, no. 10, pp. 5035-5055, 2018.

[7] M. Kamil, T. Suhartono, and Y. Ko, "Corrosion behavior of plasma electrolysis layer cross-linked with a conductive polymer coating," *Journal of Materials Research and Technology,* 2021.

[8] N. Nashrah, R. A. K. Putri, E. Z. Alharissa, W. Al Zoubi, and Y. G. Ko, "Hybrid Organic-Inorganic Materials on Metallic Surfaces: Fabrication and Electrochemical Performance," *Metals,* vol. 11, no. 7, p. 1043, 2021.

[9] E. D. Goodman, C. Zhou, and M. Cargnello, "Design of organic/inorganic hybrid catalysts for energy and environmental applications," *ACS Central Science,* vol. 6, no. 11, pp. 1916-1937, 2020.

[10] L. Jiang, J. A. Syed, H. Lu, and X. Meng, "In-situ electrodeposition of conductive polypyrrole-graphene oxide composite coating for corrosion protection of 304SS bipolar plates," *Journal of Alloys and Compounds,* vol. 770, pp. 35-47, 2019.

[11] R. M. a. M. V., "Hybrid conducting nanocomposites coatings for corrosion protection," Developments in corrosion protection, http://dx.doi.org/10.5772/57278, 2014.

[12] R. Babaei-Sati, J. B. Parsa, and M. Vakili-Azghandi, "Electrodeposition of polypyrrole/metal oxide nanocomposites for corrosion protection of mild steel—A comparative study," *Synthetic Metals,* vol. 247, pp. 183-190, 2019.

[13] T. N. Thi, T. D. T. Mai, P. T. Nam, P. N. Thu, and N. Q. Minh, "Enhanced anti-corrosion protection of carbon steel with silica-polypyrrole-dodecyl sulfate incorporated into epoxy coating," *Journal of Electronic Materials,* vol. 48, no. 6, pp. 3931-3938, 2019.

[14] Alsaad, A. M., Al-Bataineh, Q. M., Ahmad, A. A., Jum'h, I., Alaqtash, N., & Bani-Salameh, A. A. Optical properties of transparent PMMA-PS/ZnO NPs polymeric nanocomposite films: UV-Shielding applications. Materials Research Express, 6(12), 126446. 2020.

[15] A. Alsaad, A. Ahmad, A. R. Al Dairy, A. S. Al-anbar, and Q. M. Al-Bataineh, "Spectroscopic characterization of optical and thermal properties of (PMMA-PVA) hybrid thin films doped with SiO2 nanoparticles," *Results in Physics,* vol. 19, p. 103463, 2020.

[16] Jum'h, Inshad, Marwan S. Mousa, Mahmoud Mhawish, Suhad Sbeih, and Ahmad Telfah. "Optical and structural properties of (PANI‐CSA‐PMMA)/NiNPs nanocomposites thin films for organic optical filters." Journal of Applied Polymer Science 137, no. 18, p. 48643, 2020.

[17] Al-Gharram, M., Jum'h, I., Telfah, A., & Al-Hussein, M. Highly crystalline conductive electrodeposited films of PANI-CSA/CoFe2O4 nanocomposites. Colloids and Surfaces A: Physicochemical and Engineering Aspects, 628, 127342, 2021.
[18] D. Raoufi, "Journal of Luminescence," 2013.
[19] M. Rahaman, A. Aldalbahi, M. Almoiqli, and S. Alzahly, "Chemical and electrochemical synthesis of polypyrrole using carrageenan as a dopant: Polypyrrole/multi-walled carbon nanotube nanocomposites," *Polymers,* vol. 10, no. 6, p. 632, 2018.
[20] G. Sığırcık, D. Yildirim, and T. Tüken, "Synthesis and inhibitory effect of N, N'-bis (1-phenylethanol) ethylenediamine against steel corrosion in HCl Media," *Corrosion Science,* vol. 120, pp. 184-193, 2017.
[21] N. Raghavendra and J. I. Bhat, "Anti-corrosion properties of areca palm leaf extract on aluminium in 0.5 M HCl environment," *South African Journal of Chemistry,* vol. 71, pp. 30-38, 2018.
[22] A. Mirmohseni; and A. Oladegaragoze, "Anti-corrosive properties of polyaniline coating on iron," *Synthetic Metals,* vol. 114, no. 2, pp. 105-108, 2000.
[23] G. Trabanelli and V. Carassiti, "Mechanism and phenomenology of organic inhibitors," in *Advances in corrosion science and technology*: Springer, 1970, pp. 147-228.
[24] P. Singh and M. Quraishi, "Corrosion inhibition of mild steel using Novel Bis Schiff's Bases as corrosion inhibitors: electrochemical and surface measurement," *Measurement,* vol. 86, pp. 114-124, 2016.
[25] K. Ansari, M. Quraishi, and A. Singh, "Pyridine derivatives as corrosion inhibitors for N80 steel in 15% HCl: Electrochemical, surface and quantum chemical studies," *Measurement,* vol. 76, pp. 136-147, 2015.
[26] A. Y. Musa, A. A. H. Kadhum, A. B. Mohamad, and M. S. Takriff, "Experimental and theoretical study on the inhibition performance of triazole compounds for mild steel corrosion," *Corrosion Science,* vol. 52, no. 10, pp. 3331-3340, 2010.
[27] J. Zhang, X. Gong, H. Yu, and M. Du, "The inhibition mechanism of imidazoline phosphate inhibitor for Q235 steel in hydrochloric acid medium," *Corrosion science,* vol. 53, no. 10, pp. 3324-3330, 2011.
[28] L. Funes *et al.*, "Correlation between plasma antioxidant capacity and verbascoside levels in rats after oral administration of lemon verbena extract," *Food Chemistry,* vol. 117, no. 4, pp. 589-598, 2009.